



Disturbance observer–based neural adaptive fault-tolerant control for flexible air-breathing hypersonic vehicles with multiple model uncertainties

Transactions of the Institute of
Measurement and Control
1–13

© The Author(s) 2023

Article reuse guidelines:

sagepub.com/journals-permissions

DOI: 10.1177/01423312231154194

journals.sagepub.com/home/tim



Youyang Qu^{1,2,3} , Lindong Fan³, Lu Dai³, Feng Li^{1,2,3} and Xing Zhong^{1,2,3}

Abstract

One of the critical problems for flexible vehicles is how to simultaneously address the multiple uncertainty compensation and flexible vibration suppression. This paper focuses on the smooth adaptive fault-tolerant control design problem of a two-layer framework for flexible air-breathing hypersonic vehicles subject to contingent actuator failures and multiple model uncertainties. The first layer provides a disturbance observer–based neural adaptive fault-tolerant controller overcoming actuator failures and multiple model uncertainties. The second layer relies on the tracking differentiator and filter combined with the controller seamlessly, generating smooth reference information, which is highly desirable for flexible vibration suppression. Then, the analysis by the Lyapunov theory strictly proves the uniform ultimately boundedness of all the control and filter state variables. Finally, the simulation results demonstrate the dominant tracking control performance of the proposed control method.

Keywords

Flexible hypersonic vehicles, actuator failures, multiple model uncertainties, neural adaptive fault-tolerant control, smooth control action

Introduction

In the past several decades, air-breathing hypersonic vehicles have been one of the major topics to be investigated in the aerospace field for the dramatic advantages of the fastest reached and large flight envelopes (Guo et al., 2020; Xu et al., 2004). The capability of air-breathing hypersonic vehicles (AHVs) plays an important role in completing rapid near-earth orbit transportation, space exploration emergency, and global attack Guo et al. (2019a, 2019b). However, AHVs confront external disturbances and aerodynamic uncertainties due to the harsh flight environment. What's worse, the distinguishing flexible characteristic and strong coupling caused by the slender geometry is inevitable, degrading the performance of the flight control system An et al. (2021) and Ding et al. (2019a). Therefore, it is evident that the control system design of flexible air-breathing hypersonic vehicles (FAHVs) with multiple model uncertainties is not easily tackled.

The high-fidelity longitudinal model of FAHVs for the control system design has been proposed in Parker et al. (2007), where the complex dynamics functions are superseded by precise curve-fitted. Based on this model, many significant results focusing on the controller design of FAHVs have been achieved. To compensate for the vibration induced by the elastic dynamics, Wang et al. (2014) developed a coupling disturbance observer–based composite control method for FAHVs, where the generalized elastic mode coordinates are

estimated accurately. In An et al. (2016), a linear disturbance observer–based control method has been developed by utilizing the feedback linearization methodology to effectively suppress the influence of multiple uncertainties and elastic dynamics. Nevertheless, the feedback linearization model is established depending on the model parameters of actuators, which may not be available in practice. Recently, the non-linear backstepping framework has been employed to design the tracking controller by constructing a strict-feedback model of FAHVs (Sachan and Padhi, 2020). In Shao et al. (2021a), a neural network-based controller has been proposed to handle the total disturbances summarized by the influence of elastic dynamics, multiple uncertainties, and actuator failures. A similar method has been presented in Shao et al. (2021b), where the influence of elastic dynamics is regarded as a part of the lumped disturbances addressed by a convenient parameter tuning tangent function. In Ding et al. (2019b),

¹Changchun Institute of Optics, Fine Mechanics and Physics, Chinese Academy of Sciences, China

²University of Chinese Academy of Sciences, China

³Chang Guang Satellite Technology Co., Ltd., China

Corresponding author:

Xing Zhong, Changchun Institute of Optics, Fine Mechanics and Physics, Chinese Academy of Sciences, Changchun 130033, China.

Email: ciomper@163.com

the sliding mode control method has been used for designing the controller of FAHVs to deal with the multiple uncertainties, including the elastic dynamics and external disturbances. From the short review above, the flexible vibration problem caused by elastic dynamics is addressed acquiescently as a part of the lumped disturbances. It should be noted that, in addition to treating the elastic dynamics as a part of the lumped disturbances for compensation, many studies have shown that the smooth control process is highly desirable for the suppression of flexible vibration (Hu et al., 2019; Shi et al., 2020). As stated above, it is more efficient to suppress flexible vibration using active compensation combined with a smooth control process.

However, the actuator failure is considered as the primary factor for practical control system performance degrading, which even leads to instability Wang et al. (2018b) and Wang and Yuan (2019). In order to achieve reliable flight control, it is necessary to design a fault-tolerant controller for FAHVs to ensure excellent stability and control performance in the presence of contingent actuator failures. In general, the effective fault-tolerant control (FTC) method can be roughly categorized into the passive and the active control method (Argha et al., 2019; Wang et al., 2022). Different from the passive FTC method adopting the immutable control structure, the active FTC method ensures the excellent performance and stability of the considered system using the adaptive reconfigurable controller Wang et al. (2018a) and Zhang et al. (2022), which can actively compensate for actuator failures. In He et al. (2015), an output feedback adaptive control method has been proposed to compensate for the influence of actuator failures by updating the associated parameters. In Zhang et al. (2020), a second-order sliding mode observer has been constructed to estimate the lumped disturbances composed of external disturbances and actuator failures, and the higher accuracy tracking control is achieved by the observer-based nonlinear control strategy. In He et al. (2022), an adaptive feedback control method has been investigated for flight state stabilizing and vibration elimination by adaptive fault estimation. The active adaptive FTC has shown superior performance in handling actuator faults. Therefore, the adaptive FTC methodology will be inherited and carried forward for the flight control system design of FAHVs.

In this paper, a disturbance observer-based neural adaptive fault-tolerant control method is developed for FAHVs subject to contingent actuator failures and multiple model uncertainties. The neural networks are seamlessly combined with the adaptive control to compensate for actuator failures and multiple model uncertainties. The mismatched disturbances are effectively handled by introducing the nonlinear disturbance observer in this scenario. Moreover, the tracking differentiator and filter provide smooth reference information for flexible vibration suppression while reducing the complexity of the recursive control framework. To be more specific, the proposed method in this paper possesses the following features:

- A two-layer framework-based smooth neural adaptive control method is proposed to handle the complex

control problem of actuator failures, multiple model uncertainties, and elastic dynamics. The analysis by the Lyapunov theory strictly proves the uniform ultimately boundedness of all the state variables of the controller and filter.

- Unlike existing adaptive methods in He et al. (2015, 2022), this paper develops a novel neural adaptive control method to estimate the upper bounds of unknown uncertainties. Thus, strong robustness and excellent transient tracking performance are guaranteed despite time-varying actuator failures and multiple model uncertainties.
- Different from previous studies Ding et al. (2019b) and Shao et al. (2021a, 2021b) that regard the influence of elastic dynamics as a part of the lumped disturbances to compensate, this paper adopts a composite strategy to address the flexible vibration problem. The proposed design features a smooth control action that can effectively avoid exciting the major elastic dynamics by the smooth reference combined with the tangent control function. On this basis, the residual flexible vibration will be compensated by the adaptive controller.

The structure of this paper is organized as follows. The dynamic model of FAHVs subject to actuator failures and multiple model uncertainties is formulated in “Problem statement and preliminaries.” The control method and its stability analysis are given in “Main results.” The numerical analysis is given in “Simulations” to verify the dominant tracking control performance of the proposed control method. Finally, the conclusion is summarized.

Problem statement and preliminaries

Dynamic model of FAHVs

The basic structure of FAHVs is shown in Figure 1, depicting the components and variables used for attitude control. The dynamic model of generic FAHVs considered in this study is given by Parker et al. (2007), the specific form can be described as

$$\begin{aligned}
 \dot{V} &= \frac{T \cos \alpha - D}{m} - g \sin \gamma \\
 \dot{h} &= V \sin \gamma \\
 \dot{\gamma} &= \frac{L + T \sin \alpha}{mV} - \frac{g \cos \gamma}{V} \\
 \dot{\alpha} &= q - \dot{\gamma} \\
 \dot{q} &= \frac{M}{I} + \frac{\tilde{\psi}_1 \tilde{\eta}_1}{I} + \frac{\tilde{\psi}_2 \tilde{\eta}_2}{I} \\
 \ddot{\eta}_i &= -2\xi_i \omega_i \dot{\eta}_i - \omega_i^2 \eta_i + N_i + \tilde{\psi}_i \dot{q}, \quad i = 1, 2
 \end{aligned} \tag{1}$$

where the definition of related nomenclatures can be found in Appendix A. The thrust, drag, lift-force, pitching torque, and elastic force have the following expressions

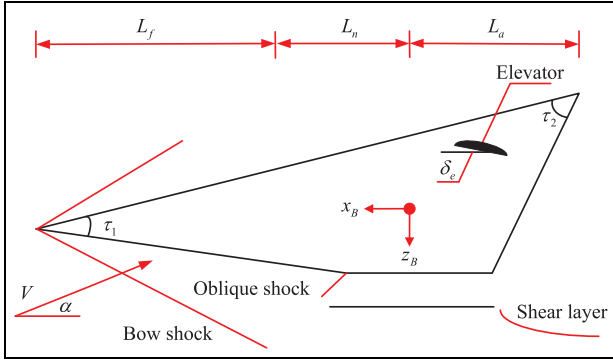


Figure 1. Geometry of FAHVs.

$$\begin{aligned}
 T &= T_0(\alpha) + T_\Phi(\alpha)\Phi + \Delta T + d_{T_e} \\
 D &= D_0 + D_\alpha(\alpha) + \Delta D + d_{D_e} \\
 L &= L_0 + L_\alpha\alpha + \Delta L + d_{L_e} \\
 M &= M_T + M_0 + M_\alpha(\alpha) + M_{\delta_e}\delta_e + \Delta M + d_{M_e} \\
 N_1 &= C_{N_1}^{\alpha^2}\alpha^2 + C_{N_1}^\alpha\alpha + C_{N_1}^0 \\
 N_2 &= C_{N_2}^{\alpha^2}\alpha^2 + C_{N_2}^\alpha\alpha + C_{N_2}^0 + C_{N_2}^{\delta_e}\delta_e
 \end{aligned} \quad (2)$$

The related variables can be further obtained according to the following equations formulated as

$$\begin{aligned}
 T_0(\alpha) &= (\beta_2\alpha^3 + \beta_4\alpha^2 + \beta_6\alpha + \beta_8) \\
 T_\Phi(\alpha) &= (\beta_1\alpha^3 + \beta_3\alpha^2 + \beta_5\alpha + \beta_7) \\
 D_0 &= \bar{q}SC_D^0, D_\alpha(\alpha) = \bar{q}S(C_D^{\alpha^2}\alpha^2 + C_D^\alpha\alpha) \\
 L_0 &= \bar{q}SC_L^0, L_\alpha = \bar{q}SC_L^\alpha \\
 M_T &= z_T T, M_{\delta_e} = \bar{q}S\bar{c}C_M^{\delta_e}, M_0 = \bar{q}S\bar{c}C_M^0 \\
 M_\alpha(\alpha) &= \bar{q}S\bar{c}(C_M^{\alpha^2}\alpha^2 + C_M^\alpha\alpha)
 \end{aligned} \quad (3)$$

Problem statement

In practical engineering, contingent actuator failures are an unavoidable problem for the flight control system, which can be decomposed into the loss of effectiveness and deviation faults Wang et al. (2018a). Thus, the time-varying actuator failures in this paper are formulated by

$$\begin{aligned}
 \Phi &= r_\Phi(t)u_\Phi + d_\Phi(t) \\
 \delta_e &= r_\delta(t)u_\delta + d_\delta(t)
 \end{aligned} \quad (4)$$

where $u_\Phi(t), u_\delta(t)$ denote the real elevator deflection and fuel equivalence ratio of FAHVs; $r_\Phi(t), r_\delta(t) \in (0, 1]$ denote the coefficient of the remanent control effectiveness, which are changing with time; and $d_\Phi(t), d_\delta(t)$ denote the time-varying deviation faults.

Moreover, the mass and inertia of FAHVs are changing with fuel consumption, which may lead to degradation of the control performance. The time-varying mass and inertia can be described as

$$\begin{aligned}
 m &= r_m(t)m_0 \\
 I &= r_I(t)I_0
 \end{aligned} \quad (5)$$

where $r_m(t)$ denotes the ratio of the real mass m to the initial mass m_0 ; $r_I(t)$ denotes the ratio of the real inertia I to the initial inertia I_0 .

Combine the velocity dynamic model of FAHVs in equation (1) with the actuator fault of the fuel equivalence ratio in equation (4) and the varying mass in equation (5), the velocity subsystem of FAHVs is derived as

$$\dot{V} = g_V\lambda_\Phi u_\Phi + f_V + d_V \quad (6)$$

where $\lambda_\Phi = r_\Phi/r_m$; the known input function g_V , the unknown model function f_V , and the lumped disturbances d_V have the following expressions

$$\begin{aligned}
 g_V &= T_\Phi \cos \alpha / m_0 \\
 f_V &= (T_0 \cos \alpha - D_0 - D_\alpha(\alpha)) / m - g \sin \gamma \\
 d_V &= ((T_\Phi d_\Phi + \Delta T + d_{T_e}) \cos \alpha - \Delta D - d_{D_e}) / m
 \end{aligned}$$

Define the state variables $x_1 = h, x_2 = \gamma, x_3 = \theta, x_4 = q$, and combine the altitude dynamic model of FAHVs in equation (1) with the actuator fault of the elevator deflection in equation (4) and the varying inertia in equation (5), the altitude subsystem of FAHVs is derived as

$$\begin{aligned}
 \dot{x}_1 &= g_1 x_2 + d_1 \\
 \dot{x}_2 &= g_2 x_3 + f_2 + d_2 \\
 \dot{x}_3 &= x_4 \\
 \dot{x}_4 &= g_4 \lambda_\delta u_\delta + f_4 + d_4
 \end{aligned} \quad (7)$$

where $\lambda_\delta = r_\delta/r_I$; $\theta = \alpha + \gamma$ denotes pitch angle; the known functions g_1, g_2, g_4, f_2 ; the unknown model function f_4 ; and the lumped disturbances d_1, d_2, d_4 have the following expressions

$$\begin{aligned}
 g_1 &= V, d_1 = V(\sin \gamma - \gamma) \\
 g_2 &= L_\alpha / (m_0 V), f_2 = -g \cos \gamma / V \\
 d_2 &= (L + T \sin \alpha) / (mV) - (L_\alpha \theta) / (m_0 V) \\
 g_4 &= M_{\delta_e} / I_0, f_4 = (M_0 + M_\alpha(\alpha)) / I \\
 d_4 &= (M_T + M_{\delta_e} d_\delta + \Delta M + d_{M_e} + \tilde{\psi}_1 \ddot{\eta}_1 + \tilde{\psi}_2 \ddot{\eta}_1) / I
 \end{aligned}$$

For the integration influence of the effectiveness loss faults and model uncertainties $\lambda_\Phi, \lambda_\delta$, the deviation faults d_δ, d_Φ , and the lumped disturbances d_V, d_1, d_2, d_4 , the following assumptions are made.

Assumption 1. Define $\Gamma_i = 1/\lambda_i, i = \delta, \Phi$. It is assumed that Γ_i is bounded. $\exists \bar{\Gamma}_i \in \mathbb{R}_+, |\Gamma_i| \leq \bar{\Gamma}_i$.

Assumption 2. For $i = 1, 2, 4, V, \delta, \Phi$, it is assumed that d_i and their derivatives \dot{d}_i are bounded. $\exists \bar{d}_i, \bar{\dot{d}}_i \in \mathbb{R}_+, |d_i| \leq \bar{d}_i, |\dot{d}_i| \leq \bar{\dot{d}}_i$.

Remark 1. $\Gamma_i, i = \delta, \Phi$ denotes the combined effect of the actuator failures, varying mass and inertia. Assumption 1 is reasonable as long as the system is not completely ineffective, which is the research premise of this paper. Moreover, Assumption 2 conforms to the fundamental laws of physics.

Preliminaries

For achieving a smooth transition process, the digital tracking differentiator in Han (2009) is used for the flight control

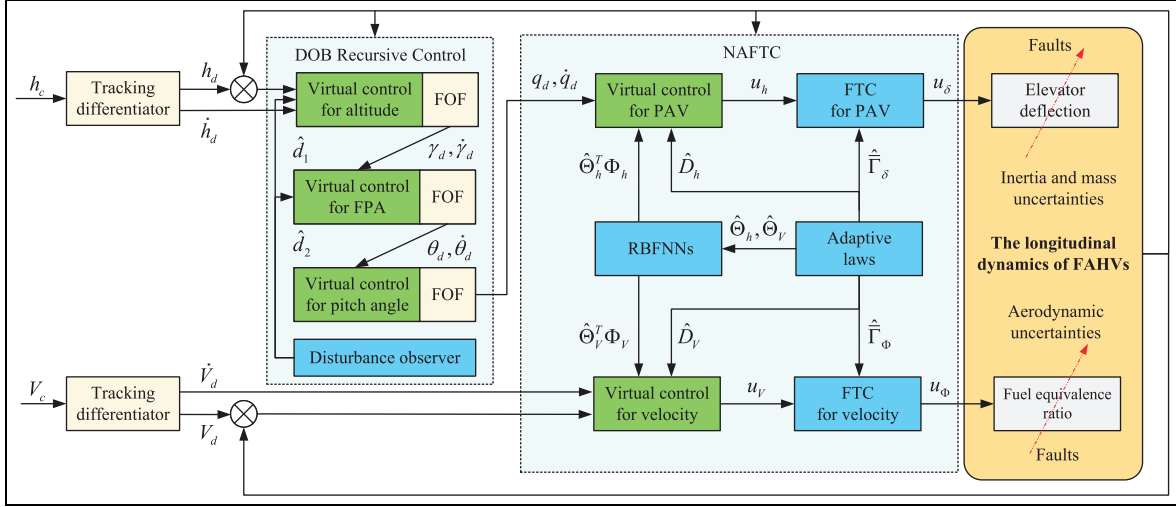


Figure 2. Structure diagram of the proposed method.

system of FAHVs to provide sufficient reference instruction information. The specific form is

$$\begin{aligned} v_1^{k+1} &= v_1^k + Sv_2^k \\ v_2^{k+1} &= v_2^k + Sa^k \end{aligned} \quad (8)$$

where v_1 and v_2 denote the design desired and its derivative, respectively; k represents the step index of the tracking differentiator; and S denotes the calculation step length. a^k is calculated as

$$\begin{aligned} a^k &= \begin{cases} -r \operatorname{sign}(a) & |a| > rS \\ -a/S & |a| \leq rS \end{cases} \\ a &= \begin{cases} v_2^k + n \operatorname{sign}(y) & |y| > rS^2 \\ v_2^k + y/S & |y| \leq rS^2 \end{cases} \\ y &= (v_1^k - v) + Sv_2^k \\ n &= 0.5 \left(\sqrt{r^2 S^2 + 8r|y|} - rS \right) \end{aligned} \quad (9)$$

where v denotes the desired step command; r denotes the convergence rate to v .

According to Lavretsky and Wise (2013) and Wang et al. (2020), the radial basis function neural networks (RBFNNs) $\Theta^T \Phi_{NN}(x)$ on a compact set $x \in \mathbb{R}^l$ can be utilized to approximate any unknown continuous function $f(x)$. The approximation results satisfy inequality as

$$\|f(x) - \Theta^T \Phi_{NN}(x)\|^2 \leq \varepsilon_{NN} \quad (10)$$

where $\varepsilon_{NN} > 0$ denotes the approximation error; $\Theta \in \mathbb{R}^l$ is an unknown constant vector denoting weights; l denotes the number of neurons, which are related to the accuracy of the approximation; and $\Phi_{NN}(x) = [\varphi_1(x), \varphi_2(x), \dots, \varphi_l(x)]^T$ denotes the radial basis function (RBF), which is a Gaussian process in the form as

$$\varphi_i(x) = e^{-\frac{\|x-c_i\|^2}{2\sigma_i^2}}, \quad i = 1, 2, \dots, l \quad (11)$$

where c_i and σ_i denote the center and the standard deviation of the isotropic Gaussian RBF components, respectively.

Lemma 1. The unknown models caused by the mass and inertia uncertainties f_V and f_4 can be approximated by the following RBFNNs

$$\begin{aligned} f_V &= \Theta_V^T \Phi_V + \varepsilon_V \\ f_4 &= \Theta_h^T \Phi_h + \varepsilon_h \end{aligned} \quad (12)$$

Lemma 2. An et al. (2020) For any $\zeta > 0$ and $m \in \mathbb{R}$, the following inequality

$$0 \leq |m| - m \tanh\left(\frac{m}{\zeta}\right) \leq \kappa \zeta \quad (13)$$

holds, where $\kappa \approx 0.2785$.

Main results

In this section, the structure diagram of the proposed method is shown in Figure 2, where the control scheme can be described in three parts. The first part uses the tracking differentiator and first-order filter (FOF) to provide smooth reference information for controller design while reducing the complexity of the recursive control framework. Hence, the smoothness and stability of tracking control are guaranteed. The second part is the disturbance observer-based recursive control, ensuring the stability of the altitude, flight path angle (FPA), and pitch angle loop by compensating for the mismatched uncertainties. The third part is the neural adaptive fault-tolerant control, achieving the stable control of the pitch angular velocity (PAV) and velocity loop subject to actuator

failures and matched uncertainties. Finally, the dominant tracking control performance is guaranteed.

Controller design for altitude subsystem

The altitude subsystem contains matched and unmatched uncertainties. To deal with the altitude control problem while avoiding the high complexity, we design the recursive neural adaptive fault-tolerant controller combined with a disturbance observer in the framework of the dynamic surface method with four steps.

Step 1. Define the altitude tracking error as $z_1 = x_1 - h_r$, the derivative of z_1 can be calculated as

$$\dot{z}_1 = g_1 x_2 + d_1 - \dot{h}_r \quad (14)$$

The control is designed to make Step 1 stable as

$$x_{2c} = -k_1 z_1 - g_1^{-1} \hat{d}_1 + g_1^{-1} \dot{h}_r \quad (15)$$

where $k_1 > 0$ denotes the control gain; \hat{d}_1 denotes the estimation of d_1 , obtained by the disturbance observer with the gain l_1 as follows

$$\begin{aligned} \dot{\hat{d}}_1 &= p_1 + l_1 z_1 \\ \dot{p}_1 &= -l_1 \hat{d}_1 - l_1 (g_1 x_2 - \dot{h}_r) \end{aligned} \quad (16)$$

Moreover, the desired for the next step x_{2d} is obtained by the first-order filter with the positive filter parameter τ_2

$$\tau_2 \dot{x}_{2d} + x_{2d} = x_{2c} - \tau_2 z_1, \quad x_{2d}(0) = x_{2c}(0) \quad (17)$$

Define $\tilde{d}_1 = \hat{d}_1 - d_1$, $y_2 = x_{2d} - x_{2c}$, and $z_2 = x_2 - x_{2d}$. Combining equations (14)–(17), we can get the error dynamics of z_1, \tilde{d}_1 , and y_2 as

$$\begin{aligned} \dot{z}_1 &= -g_1 k_1 z_1 - \tilde{d}_1 + g_1 (z_2 + y_2) \\ \dot{\tilde{d}}_1 &= -l_1 \tilde{d}_1 - \dot{d}_1 \\ \dot{y}_2 &= -\frac{y_2}{\tau_2} - z_1 - \dot{x}_{2c} \end{aligned} \quad (18)$$

Consider the following Lyapunov function candidate of Step 1

$$L_1 = \frac{1}{2g_1} z_1^2 + \frac{1}{2} \tilde{d}_1^2 + \frac{1}{2} y_2^2 \quad (19)$$

According to equation (18), the derivative of L_1 can be calculated as

$$\begin{aligned} \dot{L}_1 &\leq -\left(k_1 - \frac{1}{4g_1^2} - 1\right) z_1^2 + \frac{1}{4} z_2^2 - \left(l_1 - \frac{5}{4}\right) \tilde{d}_1^2 + \tilde{d}_1^2 \\ &\quad - \frac{y_2^2}{2\tau_2} + \frac{\tau_2 |\dot{x}_{2c}|^2}{2} \end{aligned} \quad (20)$$

Step 2. Following the similar procedure of Step 1, take the derivative of z_2 as

$$\dot{z}_2 = g_2 x_3 + f_2 + d_2 - \dot{x}_{2d} \quad (21)$$

The stable control and disturbance observer of Step 2 are designed as

$$\begin{aligned} x_{3c} &= -k_2 z_2 - g_2^{-1} (f_2 + \hat{d}_2) + g_2^{-1} \dot{x}_{2d} \\ \hat{d}_2 &= p_2 + l_2 z_2 \\ \dot{p}_2 &= -l_2 \hat{d}_2 - l_2 (g_2 x_3 + f_2 - \dot{x}_{2d}) \end{aligned} \quad (22)$$

where $k_2 > 0$ denotes the control gain; \hat{d}_2 denotes the estimation of d_2 ; and l_2 is the disturbance observer gain. The desired for the next step x_{3d} is obtained by the first-order filter with the positive filter parameter τ_3

$$\tau_3 \dot{x}_{3d} + x_{3d} = x_{3c} - \tau_3 z_2, \quad x_{3d}(0) = x_{3c}(0) \quad (23)$$

Define $\tilde{d}_2 = \hat{d}_2 - d_2$, $y_3 = x_{3d} - x_{3c}$, and $z_3 = x_3 - x_{3d}$. Combining equations (21)–(23), we can get the error dynamics of z_2, \tilde{d}_2 , and y_3 as

$$\begin{aligned} \dot{z}_2 &= -k_2 g_2 z_2 - \tilde{d}_2 + g_2 (z_3 + y_3) \\ \dot{\tilde{d}}_2 &= -l_2 \tilde{d}_2 - \dot{d}_2 \\ \dot{y}_3 &= -\frac{y_3}{\tau_3} - z_2 - \dot{x}_{3c} \end{aligned} \quad (24)$$

Consider the following Lyapunov function candidate of Step 2

$$L_2 = \frac{1}{2g_2} z_2^2 + \frac{1}{2} \tilde{d}_2^2 + \frac{1}{2} y_3^2 \quad (25)$$

According to equation (24), the derivative of L_2 can be calculated as

$$\begin{aligned} \dot{L}_2 &\leq -\left(k_2 - \frac{1}{4g_2^2} - 1\right) z_2^2 + \frac{1}{4} z_3^2 - \left(l_2 - \frac{5}{4}\right) \tilde{d}_2^2 + \tilde{d}_2^2 \\ &\quad - \frac{y_3^2}{2\tau_3} + \frac{\tau_3 |\dot{x}_{3c}|^2}{2} \end{aligned} \quad (26)$$

Step 3. Following the similar procedure of Step 1, take the derivative of z_3 as

$$\dot{z}_3 = x_4 - \dot{x}_{3d} \quad (27)$$

The control is designed to make Step 3 stable as

$$x_{4c} = -k_3 z_3 + \dot{x}_{3d} \quad (28)$$

where $k_3 > 0$ denotes the control gain. The desired for the next step x_{4d} is obtained by the first-order filter with the positive filter parameter τ_4

$$\tau_4 \dot{x}_{4d} + x_{4d} = x_{4c} - \tau_4 z_3, \quad x_{4d}(0) = x_{4c}(0) \quad (29)$$

Define $y_4 = x_{4d} - x_{4c}$ and $z_4 = x_4 - x_{4d}$. Combining equations (27)–(29), we can get the error dynamics of z_3 and y_4 as

$$\begin{aligned} \dot{z}_3 &= -k_3 z_3 + (z_4 + y_4) \\ \dot{y}_4 &= -\frac{y_4}{\tau_4} - z_3 - \dot{x}_{4c} \end{aligned} \quad (30)$$

Consider the following Lyapunov function candidate of Step 3

$$L_3 = \frac{1}{2}z_3^2 + \frac{1}{2}y_4^2 \quad (31)$$

According to equation (30), the derivative of L_3 can be calculated as

$$\dot{L}_3 \leq -(k_3 - 1)z_3^2 + \frac{1}{4}z_4^2 - \frac{y_4^2}{2\tau_4} + \frac{\tau_4|\dot{x}_{4c}|^2}{2} \quad (32)$$

Step 4. Take the derivative of z_4 as

$$\dot{z}_4 = g_4\lambda_\delta u_\delta + f_4 + d_4 - \dot{x}_{4d} \quad (33)$$

According to Lemma 1, the unknown model f_4 caused by the inertia uncertainty can be approximated by the RBFNNs $f_4 = \Theta_h^T \Phi_h + \varepsilon_h$. Thus, the control is designed to make Step 4 stable as

$$u_h = -k_4 z_4 - \hat{D}_h \tanh\left(\frac{z_4}{\varepsilon_{D_h}}\right) - \hat{\Theta}_h^T \Phi_h + \dot{x}_{4d} \quad (34)$$

where $D_h = \bar{d}_h$, $d_h = d_4 + \varepsilon_h$, and $\hat{D}_h, \hat{\Theta}_h$ denote the estimation of D_h, Θ_h , and $\tilde{D}_h = \hat{D}_h - D_h$ and $\tilde{\Theta}_h = \hat{\Theta}_h - \Theta_h$ denote the estimation errors, respectively.

Substituting equation (34) into equation (33), the \dot{z}_4 can be written as

$$\dot{z}_4 = -k_4 z_4 - \hat{D}_h \tanh\left(\frac{z_4}{\varepsilon_{D_h}}\right) + d_h + g_4\lambda_\delta u_\delta - u_h - \tilde{\Theta}_h^T \Phi_h \quad (35)$$

Finally, the actual control action of the altitude subsystem is designed as

$$u_\delta = -\frac{\hat{\Gamma}_\delta u_h \tanh\left(\frac{z_4 \hat{\Gamma}_\delta u_h}{\varepsilon_{\hat{\Gamma}_\delta}}\right)}{g_4} \quad (36)$$

with the adaptive laws are designed as

$$\begin{aligned} \dot{\hat{D}}_h &= K_{D_h} z_4 \tanh\left(\frac{z_4}{\varepsilon_{D_h}}\right) - \sigma_{D_h} \hat{D}_h \\ \dot{\hat{\Gamma}}_\delta &= -K_{\hat{\Gamma}_\delta} z_4 u_h - \sigma_{\hat{\Gamma}_\delta} \hat{\Gamma}_\delta \\ \dot{\hat{\Theta}}_h &= K_{\Theta_h} z_4 \Phi_h - \sigma_{\Theta_h} \hat{\Theta}_h \end{aligned} \quad (37)$$

where $\hat{\Gamma}_\delta$ denotes the estimation of $\bar{\Gamma}_\delta$, and $\tilde{\Gamma}_\delta = \hat{\Gamma}_\delta - \bar{\Gamma}_\delta$ denotes the estimation error; ε_{D_h} and $\varepsilon_{\hat{\Gamma}_\delta}$ are the design positive constants; σ_{D_h} , $\sigma_{\hat{\Gamma}_\delta}$, and σ_{Θ_h} are the positive modifying constants of the adaptive laws; and K_{D_h} , $K_{\hat{\Gamma}_\delta}$ and K_{Θ_h} are the gain of the adaptive laws.

Consider the following Lyapunov function candidate of Step 4

$$L_4 = \frac{1}{2}z_4^2 + \frac{1}{2K_{D_h}}\tilde{D}_h^2 + \frac{1}{2K_{\hat{\Gamma}_\delta}\bar{\Gamma}_\delta}\tilde{\Gamma}_\delta^2 + \frac{1}{2K_{\Theta_h}}\tilde{\Theta}_h^T \tilde{\Theta}_h \quad (38)$$

According to equation (35), the derivative of L_4 can be calculated as

$$\begin{aligned} \dot{L}_4 &= -k_4 z_4^2 - z_4 \hat{D}_h \tanh\left(\frac{z_4}{\varepsilon_{D_h}}\right) + z_4 d_h + z_4 g_4 \lambda_\delta u_\delta \\ &\quad - z_4 u_h - z_4 \tilde{\Theta}_h^T \Phi_h + \frac{\tilde{D}_h \dot{\tilde{D}}_h}{K_{D_h}} + \frac{\tilde{\Gamma}_\delta \dot{\tilde{\Gamma}}_\delta}{K_{\hat{\Gamma}_\delta} \bar{\Gamma}_\delta} + \frac{\tilde{\Theta}_h^T \dot{\tilde{\Theta}}_h}{K_{\Theta_h}} \end{aligned} \quad (39)$$

Using Lemma 2, it is easy to obtain that

$$\begin{aligned} z_4 d_h &\leq D_h z_4 \tanh\left(\frac{z_4}{\varepsilon_{D_h}}\right) + \kappa D_h \varepsilon_{D_h} \\ z_4 g_4 \lambda_\delta u_\delta &\leq \frac{\hat{\Gamma}_\delta}{\bar{\Gamma}_\delta} z_4 u_h + \frac{\kappa \varepsilon_{\hat{\Gamma}_\delta}}{\bar{\Gamma}_\delta} \end{aligned} \quad (40)$$

Furthermore, we can get

$$\begin{aligned} z_4 d_h - z_4 \hat{D}_h \tanh\left(\frac{z_4}{\varepsilon_{D_h}}\right) &\leq -z_4 \tilde{D}_h \tanh\left(\frac{z_4}{\varepsilon_{D_h}}\right) + \kappa D_h \varepsilon_{D_h} \\ z_4 g_4 \lambda_\delta u_\delta - z_4 u_h &\leq \frac{\tilde{\Gamma}_\delta}{\bar{\Gamma}_\delta} z_4 u_h + \frac{\kappa \varepsilon_{\hat{\Gamma}_\delta}}{\bar{\Gamma}_\delta} \end{aligned} \quad (41)$$

Substituting equation (41) into equation (39), we can obtain that

$$\begin{aligned} \dot{L}_4 &\leq -k_4 z_4^2 + \tilde{D}_h \left(\frac{\dot{\tilde{D}}_h}{K_{D_h}} - z_4 \tanh\left(\frac{z_4}{\varepsilon_{D_h}}\right) \right) + \frac{\tilde{\Gamma}_\delta}{\bar{\Gamma}_\delta} \left(\frac{\dot{\tilde{\Gamma}}_\delta}{K_{\hat{\Gamma}_\delta}} + z_4 u_h \right) \\ &\quad + \tilde{\Theta}_h^T \left(\frac{\dot{\tilde{\Theta}}_h}{K_{\Theta_h}} - z_4 \Phi_h \right) + \kappa D_h \varepsilon_{D_h} + \frac{\kappa \varepsilon_{\hat{\Gamma}_\delta}}{\bar{\Gamma}_\delta} \end{aligned} \quad (42)$$

According to the adaptive laws in equation (37), equation (42) can be formulated into

$$\dot{L}_4 \leq -k_4 z_4^2 - \frac{\sigma_{D_h} \tilde{D}_h \dot{\tilde{D}}_h}{K_{D_h}} - \frac{\sigma_{\hat{\Gamma}_\delta} \tilde{\Gamma}_\delta \dot{\tilde{\Gamma}}_\delta}{K_{\hat{\Gamma}_\delta} \bar{\Gamma}_\delta} - \frac{\sigma_{\Theta_h} \tilde{\Theta}_h^T \dot{\tilde{\Theta}}_h}{K_{\Theta_h}} + \kappa D_h \varepsilon_{D_h} + \frac{\kappa \varepsilon_{\hat{\Gamma}_\delta}}{\bar{\Gamma}_\delta} \quad (43)$$

Using Young's inequality Young (1912) we can get

$$\begin{aligned} -\frac{\sigma_{D_h} \tilde{D}_h \dot{\tilde{D}}_h}{K_{D_h}} &\leq -\frac{\sigma_{D_h} \tilde{D}_h^2}{2K_{D_h}} + \frac{\sigma_{D_h} D_h^2}{2K_{D_h}} \\ -\frac{\sigma_{\hat{\Gamma}_\delta} \tilde{\Gamma}_\delta \dot{\tilde{\Gamma}}_\delta}{K_{\hat{\Gamma}_\delta} \bar{\Gamma}_\delta} &\leq -\frac{\sigma_{\hat{\Gamma}_\delta} \tilde{\Gamma}_\delta^2}{2K_{\hat{\Gamma}_\delta} \bar{\Gamma}_\delta} + \frac{\sigma_{\hat{\Gamma}_\delta} \bar{\Gamma}_\delta^2}{2K_{\hat{\Gamma}_\delta} \bar{\Gamma}_\delta} \\ -\frac{\sigma_{\Theta_h} \tilde{\Theta}_h^T \dot{\tilde{\Theta}}_h}{K_{\Theta_h}} &\leq -\frac{\sigma_{\Theta_h} \tilde{\Theta}_h^T \tilde{\Theta}_h}{2K_{\Theta_h}} + \frac{\sigma_{\Theta_h} \Theta_h^T \Theta_h}{2K_{\Theta_h}} \end{aligned} \quad (44)$$

Substituting equation (44) into equation (43), we can obtain that

$$\begin{aligned} \dot{L}_4 &\leq -k_4 z_4^2 - \frac{\sigma_{D_h} \tilde{D}_h^2}{2K_{D_h}} - \frac{\sigma_{\hat{\Gamma}_\delta} \tilde{\Gamma}_\delta^2}{2K_{\hat{\Gamma}_\delta} \bar{\Gamma}_\delta} - \frac{\sigma_{\Theta_h} \tilde{\Theta}_h^T \tilde{\Theta}_h}{2K_{\Theta_h}} + \frac{\sigma_{D_h} D_h^2}{2K_{D_h}} \\ &\quad + \frac{\sigma_{\hat{\Gamma}_\delta} \bar{\Gamma}_\delta^2}{2K_{\hat{\Gamma}_\delta} \bar{\Gamma}_\delta} + \frac{\sigma_{\Theta_h} \Theta_h^T \Theta_h}{2K_{\Theta_h}} + \kappa D_h \varepsilon_{D_h} + \frac{\kappa \varepsilon_{\hat{\Gamma}_\delta}}{\bar{\Gamma}_\delta} \end{aligned} \quad (45)$$

Theorem 1. For the altitude subsystem in equation (7), let the recursive controller in equations (15), (22), (28) and (36), and the adaptive laws in equation (37) be applied. Then the uniform ultimate boundedness of the altitude subsystem is guaranteed.

Proof. Consider the following Lyapunov function of the altitude subsystem

$$L_h = \sum_{i=1}^4 L_i \quad (46)$$

where L_i is defined in equations (19), (25), (31), and (38). According to the derivative calculation results of the Lyapunov candidate functions in equations (20), (26), (32), and (45), the derivative of L_h can be calculated as

$$\begin{aligned} \dot{L}_h \leq & - \left(k_1 - \frac{1}{4g_1^2} - 1 \right) z_1^2 - \left(k_2 - \frac{1}{4g_2^2} - \frac{5}{4} \right) z_2^2 - \left(k_3 - \frac{5}{4} \right) z_3^2 \\ & - \left(k_4 - \frac{1}{4} \right) z_4^2 - \left(l_1 - \frac{5}{4} \right) \tilde{d}_1^2 \\ & - \left(l_2 - \frac{5}{4} \right) \tilde{d}_2^2 - \frac{y_2^2}{2\tau_2} - \frac{y_3^2}{2\tau_3} - \frac{y_4^2}{2\tau_4} - \frac{\sigma_{D_h} \tilde{D}_h^2}{2K_{D_h}} - \frac{\sigma_{\Gamma_\delta} \tilde{\Gamma}_\delta^2}{2K_{\Gamma_\delta}} \\ & - \frac{\sigma_{\Theta_h} \tilde{\Theta}_h^T \tilde{\Theta}_h}{2K_{\Theta_h}} + \varepsilon_{L_h} \end{aligned} \quad (47)$$

where

$$\begin{aligned} \varepsilon_{L_h} = & \bar{d}_1^2 + \bar{d}_2^2 + \frac{\tau_2 |\dot{x}_{2c}|^2}{2} + \frac{\tau_3 |\dot{x}_{3c}|^2}{2} + \frac{\tau_4 |\dot{x}_{4c}|^2}{2} + \frac{\sigma_{D_h} D_h^2}{2K_{D_h}} \\ & + \frac{\sigma_{\Gamma_\delta} \bar{\Gamma}_\delta^2}{2K_{\Gamma_\delta}} + \frac{\sigma_{\Theta_h} \Theta_h^T \Theta_h}{2K_{\Theta_h}} + \kappa D_h \varepsilon_{D_h} + \frac{\kappa \varepsilon_{\Gamma_\delta}}{\bar{\Gamma}_\delta} \end{aligned} \quad (48)$$

Furthermore, we have the following conclusion

$$\dot{L}_h \leq -\mu_h L_h + \bar{\varepsilon}_{L_h} \quad (49)$$

where

$$\mu_h = \min \left(2g_1 \left(k_1 - \frac{1}{4g_1^2} - 1 \right), 2g_2 \left(k_2 - \frac{1}{4g_2^2} - \frac{5}{4} \right), 2 \left(k_3 - \frac{5}{4} \right), 2 \left(k_4 - \frac{1}{4} \right), \right. \\ \left. 2 \left(l_1 - \frac{5}{4} \right), 2 \left(l_2 - \frac{5}{4} \right), \frac{1}{\tau_2}, \frac{1}{\tau_3}, \frac{1}{\tau_4}, \sigma_{D_h}, \sigma_{\Gamma_\delta}, \sigma_{\Theta_h} \right) \quad (50)$$

It is clear that $\forall t \geq 0, 0 \leq L_h(t) \leq \max \left\{ \frac{\bar{\varepsilon}_{L_h}}{2\mu_h}, L_h(0) \right\}$. Therefore, the uniform ultimate boundedness of the altitude subsystem can be guaranteed.

Controller design for velocity subsystem

Define the velocity tracking error as $z_V = V - V_r$, the derivative of z_V can be calculated as

$$\dot{z}_V = g_V \lambda_\Phi u_\Phi + f_V + d_V - \dot{V}_r \quad (51)$$

According to Lemma 1, the unknown model f_V caused by the mass uncertainty can be approximated by the RBFNNs $f_V = \Theta_V^T \Phi_V + \varepsilon_V$. Thus, the virtual control of the velocity subsystem is designed as

$$u_V = -k_V z_V - \hat{D}_V \tanh \left(\frac{z_V}{\varepsilon_{D_V}} \right) - \hat{\Theta}_V^T \Phi_V + \dot{V}_r \quad (52)$$

where $D_V = \bar{d}_{V_i}$, $d_{V_i} = d_V + \varepsilon_V$, $\hat{D}_V, \hat{\Theta}_V$ denote the estimation of D_V, Θ_V , and $\tilde{D}_V = \hat{D}_V - D_V, \tilde{\Theta}_V = \hat{\Theta}_V - \Theta_V$ denote the estimation errors, respectively.

Substituting equation (52) into equation (51), the \dot{z}_V can be written as

$$\dot{z}_V = -k_V z_V - \hat{D}_V \tanh \left(\frac{z_V}{\varepsilon_{D_V}} \right) + d_V + g_V \lambda_\Phi u_\Phi - u_V - \tilde{\Theta}_V^T \Phi_V \quad (53)$$

Finally, the actual control action of the altitude subsystem is designed as

$$u_\Phi = -\frac{\hat{\Gamma}_\Phi u_V}{g_V} \tanh \left(\frac{z_V \hat{\Gamma}_\Phi u_V}{\varepsilon_{\Gamma_\Phi}} \right) \quad (54)$$

with the adaptive laws are designed as

$$\begin{aligned} \dot{\hat{D}}_V &= K_{D_V} z_V \tanh \left(\frac{z_V}{\varepsilon_{D_V}} \right) - \sigma_{D_V} \hat{D}_V \\ \dot{\hat{\Gamma}}_\Phi &= -K_{\Gamma_\Phi} z_V u_V - \sigma_{\Gamma_\Phi} \hat{\Gamma}_\Phi \\ \dot{\hat{\Theta}}_V &= K_{\Theta_V} z_V \Phi_V - \sigma_{\Theta_V} \hat{\Theta}_V \end{aligned} \quad (55)$$

where $\hat{\Gamma}_\Phi$ denotes the estimation of $\bar{\Gamma}_\Phi$, and $\tilde{\Gamma}_\Phi = \hat{\Gamma}_\Phi - \bar{\Gamma}_\Phi$ denotes the estimation error; ε_{D_V} and $\varepsilon_{\Gamma_\Phi}$ are the design positive constants; $\sigma_{D_V}, \sigma_{\Gamma_\Phi}$, and σ_{Θ_V} are the positive modifying constants of the adaptive laws; K_{D_V}, K_{Γ_Φ} , and K_{Θ_V} are the gain of the adaptive laws.

Theorem 2. For the velocity subsystem in equation (6), let the controller in equation (54) and the adaptive laws in equation (55) be applied. Then the uniform ultimate boundedness of the velocity subsystem is guaranteed.

Proof. Consider the following Lyapunov function of the velocity subsystem

$$L_V = \frac{1}{2} z_V^2 + \frac{1}{2K_{D_V}} \tilde{D}_V^2 + \frac{1}{2K_{\Gamma_\Phi} \bar{\Gamma}_\Phi} \tilde{\Gamma}_\Phi^2 + \frac{1}{2K_{\Theta_V}} \tilde{\Theta}_V^T \tilde{\Theta}_V \quad (56)$$

According to equation (53), we can obtain the derivative of L_V as

$$\begin{aligned} \dot{L}_V = & -k_V z_V^2 - z_V \hat{D}_V \tanh \left(\frac{z_V}{\varepsilon_{D_V}} \right) + z_V d_V + z_V g_V \lambda_\Phi u_\Phi \\ & - z_V u_V - z_V \tilde{\Theta}_V^T \Phi_V \\ & + \frac{\tilde{D}_V \dot{\tilde{D}}_V}{K_{D_V}} + \frac{\tilde{\Gamma}_\Phi \dot{\tilde{\Gamma}}_\Phi}{K_{\Gamma_\Phi} \bar{\Gamma}_\Phi} + \frac{\tilde{\Theta}_V^T \dot{\tilde{\Theta}}_V}{K_{\Theta_V}} \end{aligned} \quad (57)$$

Using Lemma 2, it is easy to obtain that

$$\begin{aligned} z_V d_{V_i} &\leq D_V z_V \tanh\left(\frac{z_V}{\varepsilon_{D_V}}\right) + \kappa D_V \varepsilon_{D_V} \\ z_V g_V \lambda_{\Phi} u_{\Phi} &\leq \frac{\hat{\Gamma}_{\Phi}}{\bar{\Gamma}_{\Phi}} z_V u_V + \frac{\kappa \varepsilon_{\hat{\Gamma}_{\Phi}}}{\bar{\Gamma}_{\Phi}} \end{aligned} \quad (58)$$

Furthermore, we can get

$$\begin{aligned} z_V d_{V_i} - z_V \hat{D}_V \tanh\left(\frac{z_V}{\varepsilon_{D_V}}\right) &\leq -z_V \tilde{D}_V \tanh\left(\frac{z_V}{\varepsilon_{D_V}}\right) + \kappa D_V \varepsilon_{D_V} \\ z_V g_V \lambda_{\Phi} u_{\Phi} - z_V u_V &\leq \frac{\tilde{\Gamma}_{\Phi}}{\bar{\Gamma}_{\Phi}} z_V u_V + \frac{\kappa \varepsilon_{\tilde{\Gamma}_{\Phi}}}{\bar{\Gamma}_{\Phi}} \end{aligned} \quad (59)$$

Substituting equation (59) into equation (57), we can obtain

$$\begin{aligned} \dot{L}_V &= -k_V z_V^2 + \tilde{D}_V \left(\frac{\dot{D}_V}{K_{D_V}} - z_V \tanh\left(\frac{z_V}{\varepsilon_{D_V}}\right) \right) \\ &+ \frac{\tilde{\Gamma}_{\Phi}}{\bar{\Gamma}_{\Phi}} \left(\frac{\dot{\Gamma}_{\Phi}}{K_{\Gamma_{\Phi}}} + z_V u_V \right) + \tilde{\Theta}_V^T \left(\frac{\dot{\Theta}_V}{K_{\Theta_V}} - z_V \Phi_V \right) \\ &+ \kappa D_V \varepsilon_{D_V} + \frac{\kappa \varepsilon_{\tilde{\Gamma}_{\Phi}}}{\bar{\Gamma}_{\Phi}} \end{aligned} \quad (60)$$

According to the adaptive laws in equation (55), equation (60) can be formulated into

$$\begin{aligned} \dot{L}_V &\leq -k_V z_V^2 - \frac{\sigma_{D_V} \tilde{D}_V \hat{D}_V}{K_{D_V}} - \frac{\sigma_{\tilde{\Gamma}_{\Phi}} \tilde{\Gamma}_{\Phi} \hat{\Gamma}_{\Phi}}{K_{\tilde{\Gamma}_{\Phi}} \bar{\Gamma}_{\Phi}} - \frac{\sigma_{\Theta_V} \tilde{\Theta}_V^T \hat{\Theta}_V}{K_{\Theta_V}} \\ &+ \kappa D_V \varepsilon_{D_V} + \frac{\kappa \varepsilon_{\tilde{\Gamma}_{\Phi}}}{\bar{\Gamma}_{\Phi}} \end{aligned} \quad (61)$$

Using Young's inequality we can get

$$\begin{aligned} -\frac{\sigma_{D_V} \tilde{D}_V \hat{D}_V}{K_{D_V}} &\leq -\frac{\sigma_{D_V} \tilde{D}_V^2}{2K_{D_V}} + \frac{\sigma_{D_V} D_V^2}{2K_{D_V}} \\ -\frac{\sigma_{\tilde{\Gamma}_{\Phi}} \tilde{\Gamma}_{\Phi} \hat{\Gamma}_{\Phi}}{K_{\tilde{\Gamma}_{\Phi}} \bar{\Gamma}_{\Phi}} &\leq -\frac{\sigma_{\tilde{\Gamma}_{\Phi}} \tilde{\Gamma}_{\Phi}^2}{2K_{\tilde{\Gamma}_{\Phi}} \bar{\Gamma}_{\Phi}} + \frac{\sigma_{\tilde{\Gamma}_{\Phi}} \bar{\Gamma}_{\Phi}^2}{2K_{\tilde{\Gamma}_{\Phi}} \bar{\Gamma}_{\Phi}} \\ -\frac{\sigma_{\Theta_V} \tilde{\Theta}_V^T \hat{\Theta}_V}{K_{\Theta_V}} &\leq -\frac{\sigma_{\Theta_V} \tilde{\Theta}_V^T \tilde{\Theta}_V}{2K_{\Theta_V}} + \frac{\sigma_{\Theta_V} \Theta_V^T \Theta_V}{2K_{\Theta_V}} \end{aligned} \quad (62)$$

Substituting equation (62) into equation (61), we can get the following inequality

$$\dot{L}_V \leq -k_V z_V^2 - \frac{\sigma_{D_V} \tilde{D}_V^2}{2K_{D_V}} - \frac{\sigma_{\tilde{\Gamma}_{\Phi}} \tilde{\Gamma}_{\Phi}^2}{2K_{\tilde{\Gamma}_{\Phi}} \bar{\Gamma}_{\Phi}} - \frac{\sigma_{\Theta_V} \tilde{\Theta}_V^T \tilde{\Theta}_V}{2K_{\Theta_V}} + \varepsilon_{L_V} \quad (63)$$

where

$$\varepsilon_{L_V} = \frac{\sigma_{D_V} D_V^2}{2K_{D_V}} + \frac{\sigma_{\tilde{\Gamma}_{\Phi}} \bar{\Gamma}_{\Phi}^2}{2K_{\tilde{\Gamma}_{\Phi}} \bar{\Gamma}_{\Phi}} + \frac{\sigma_{\Theta_V} \Theta_V^T \Theta_V}{2K_{\Theta_V}} + \kappa D_V \varepsilon_{D_V} + \frac{\kappa \varepsilon_{\tilde{\Gamma}_{\Phi}}}{\bar{\Gamma}_{\Phi}} \quad (64)$$

Furthermore, we have the following conclusion

$$\dot{L}_V \leq -\mu_V L_V + \bar{\varepsilon}_{L_V} \quad (65)$$

where

$$\mu_V = \min\{2k_V, \sigma_{D_V}, \sigma_{\tilde{\Gamma}_{\Phi}}, \sigma_{\Theta_V}\} \quad (66)$$

It is clear that $\forall t \geq 0, 0 \leq L_V(t) \leq \max\left\{\frac{\bar{\varepsilon}_{L_V}}{2\mu_V}, L_V(0)\right\}$. Therefore, the uniform ultimate boundedness of the velocity subsystem can be guaranteed.

Simulations

This section presents several simulations to demonstrate the effectiveness and robustness of the proposed neural adaptive fault-tolerant controller (NAFTC). To be more persuasive, the feedback linearization-based linear quadratic regulator (FLLQR) and the disturbance observer-based controller (DOBC) in An et al. (2016) and Shao et al. (2021a) are applied in simulations for comparison. The LQR controller is among the most used controller of vehicles for its simplicity and applicability. The DOBC method and so on mentioned above repeatedly is widely used to deal with actuator faults and multiple uncertainties of FAHVs. Both methods rely on the linearized model as

$$\dot{x} = \mathbf{A}x + \mathbf{B}u + \hat{d}_l \quad (67)$$

where the state variable x , state matrix \mathbf{A} , and control matrix \mathbf{B} are defined in An et al. (2016).

The specific form of the LQR is

$$u_{lqr} = -\mathbf{K}_{lqr}x \quad (68)$$

with the optimal feedback gain \mathbf{K}_{lqr} calculated to minimize the following energy function

$$L = \frac{1}{2} \int_0^t [x^T \mathbf{Q}x + u^T \mathbf{R}u] dt \quad (69)$$

where \mathbf{Q} and \mathbf{R} are the diagonal positive definite weight matrices. The larger the weight matrices, the smaller the desired error of x and control energy u , respectively.

The specific form of the DOBC is

$$\begin{aligned} u_{dobe} &= -\mathbf{K}_x x - \mathbf{K}_d \hat{d}_l \\ \hat{d}_l &= \mathbf{p} + \mathbf{L}_d x \\ \dot{\mathbf{p}} &= -\mathbf{L}_d (\mathbf{p} + \mathbf{L}_d x) - \mathbf{L}_d (\mathbf{A}x + \mathbf{B}u) \end{aligned} \quad (70)$$

where \mathbf{K}_x , \mathbf{K}_d , and \mathbf{L}_d are the control gain matrix, the disturbance compensation gain matrix, and the disturbance observer gain matrix, which are both calculated by pole assignment, respectively; and \hat{d}_l is the estimation of the lumped disturbance d_l .

Control parameters setting

The vehicle parameters and the aerodynamic coefficients of simulations can be found in Parker et al. (2007). The initial and desired conditions of the system states are given in Table 1. The initial values of angle of attack (AOA) and FAV are set as random values to verify the robustness of

Table 1. Initial and desired conditions of the system states.

	Velocity, V (ft/s)	Altitude, h (ft)	FPA, γ (deg)	AOA, α (deg)	PAV, q (deg/s)
Initial value	7700	80,000	0	1	4
Desired value	8500	90,000	–	–	–

FPA: flight path angle; AOA: angle of attack; PAV: pitch angular velocity.

Table 2. Parameters of the proposed control method.

Altitude subsystem			Velocity subsystem		
Parameter	Value	Parameter	Value	Parameter	Value
k_1	$0.4/g_1$	K_{D_h}	1	k_V	0.4
k_2	$0.7/g_2$	K_{Γ_δ}	1	K_{D_V}	1
k_3	1.1	K_{Θ_h}	10	K_{Γ_Φ}	0.5
k_4	100	$\sigma_{D_h}, \sigma_{\Gamma_\delta}$	0.2	K_{Θ_V}	10
l_1	0.1	σ_{Θ_h}	0.5	$\sigma_{D_V}, \sigma_{\Gamma_\Phi}$	0.1
l_2	0.2	$\varepsilon_{\Gamma_\delta}$	0.005	σ_{Θ_V}	0.5
ε_{D_h}	0.01	τ_2	0.5	$\varepsilon_{D_V}, \varepsilon_{\Gamma_\Phi}$	0.1
τ_3	0.1	τ_4	0.03	r_V	0.1
r_h	1.5	σ_h	0.2	σ_V	1
c_h	$[-0.2, -0.1, 0, 0.1, 0.2]$			c_V	$[-2, -1, 0, 1, 2]$

the proposed method. The references of V_r, \dot{V}_r and h_r, \dot{h}_r are derived from filtering step commands by the tracking differentiator, with the parameter r_V for the velocity subsystem, and r_h for the altitude subsystem. The number of neurons for two subsystems is five, with the RBFNNs parameters c_V and σ_V for the velocity subsystem, and c_h and σ_h for the altitude subsystem. All parameters of the proposed control method are given in Table 2. In addition, the control parameters of LQR are $Q = \text{diag}(10, 1, 1, 1, 1, 1, 1)$ and $R = \text{diag}(1, 0.1)$; the control parameters of DOBC are

$$\mathbf{K}_x = \begin{bmatrix} 0.68 & 3.42 & 7.75 & 0 & 0 & 0 & 0 \\ 0 & 0 & 0 & 0.034 & 1.62 & 1.53 & 9.43 \end{bmatrix},$$

$$\mathbf{K}_d = \begin{bmatrix} 3.42 & 7.75 & 1 & 0 & 0 & 0 & 0 \\ 0 & 0 & 0 & 1.62 & 1.53 & 9.43 & 1 \end{bmatrix}, \quad \text{and}$$

$$\mathbf{L}_d = \begin{bmatrix} \text{diag}(10, 10, 10) & \mathbf{0}_{3 \times 4} \\ \mathbf{0}_{4 \times 3} & \text{diag}(6, 2, 2, 2) \end{bmatrix}.$$

Simulation results

In order to analyze the control performance of the proposed method and the comparison methods, the simulations are implemented in two cases. In Case 1, the simulation results of FAHVs with fixed actuator failures and multiple uncertainties are given to illustrate the excellent tracking performance of the proposed method. In Case 2, the simulation results of FAHVs with more complex time-varying actuator failures, multiple uncertainties and measurement noises are given to illustrate the superior robustness of the proposed method.

Case 1: The fixed actuator failures occur at $t = 100$ s with parameters $r_\delta = 0.79, r_\Phi = 0.75, d_\delta = 0.09, d_\Phi = 0.08$, and change at $t = 300$ s with parameters $r_\delta = 0.74, r_\Phi = 0.71, d_\delta = 0.15, d_\Phi = 0.11$. The multiple model uncertainties include -30% deviations of aerodynamic parameters and -10% deviations of mass and inertia. The external disturbances and measurement noise are not considered.

The simulation results of Case 1 are presented in Figures 3–8. The velocity and altitude tracking performance are depicted in Figures 3 and 4. It is clear that the velocity and altitude of NAFTC rapidly convergence to the reference when the climbing flight is beginning. In contrast, the convergence rate of the two other comparison methods is relatively slow. In other words, NAFTC has the best transient control characteristics. Moreover, whether before or after actuator failures, the velocity and altitude errors of NAFTC are less than 0.3ft/s and 3.5ft, respectively. When it comes to the velocity and altitude errors of FLLQR are 18.1ft/s and 89ft, and DOBC are 9.7ft/s and 25.8ft. The attitude states are depicted in Figure 5. When actuator failures occur, the attitude states of FLLQR and DOBC fluctuate violently, and NAFTC remains stable. The elastic mode coordinates are depicted in Figure 6. Due to the impact of the first actuator failure, it is obvious that the elastic mode coordinates of FLLQR and DOBC oscillate for the excited flexible vibration. In contrast, owing to the smooth control, the oscillation amplitude of NAFTC is less than the treble of the two other comparison methods. The control actions are depicted in Figure 7, the estimation results of the disturbance observers

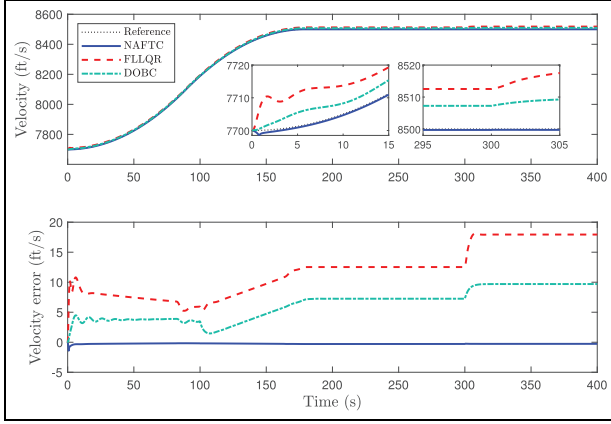


Figure 3. Velocity tracking performance in Case 1.

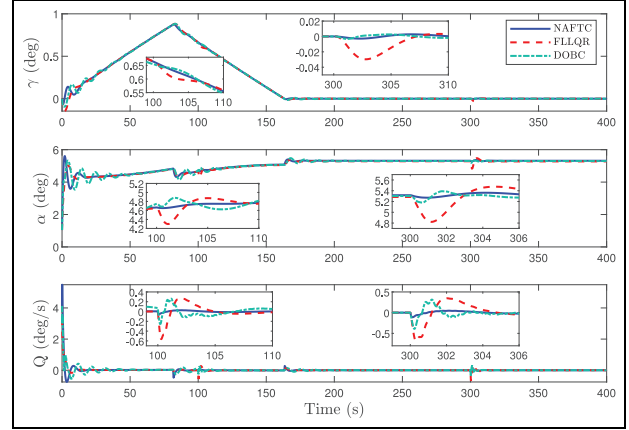


Figure 5. Attitude state in Case 1.

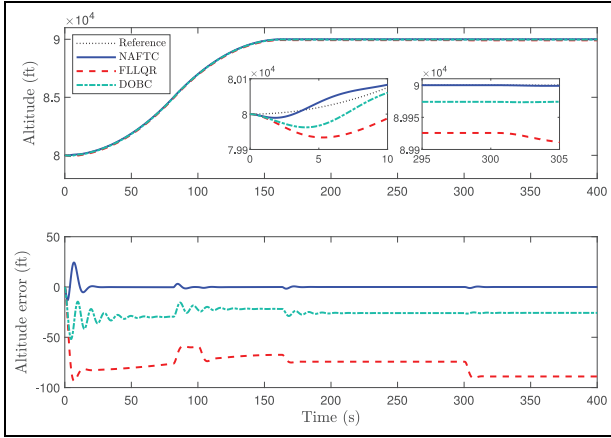


Figure 4. Altitude tracking performance in Case 1.

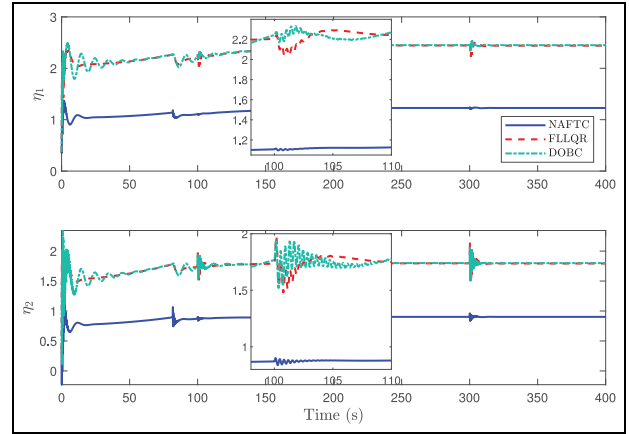


Figure 6. Elastic mode coordinate in Case 1.

and adaptive laws are depicted in Figure 8. From Figures 7 and 8, it is interesting to note that the quick control action and the accurate estimation of the unknown terms are important for the excellent control performance of the proposed control method.

In general, in terms of the control accuracy, the response agility for contingent actuator failures, and the flexible vibration suppression, NAFTC ensures the highest degree, DOBC followed and FLLQR worst.

Case 2: The time-varying actuator failures occur at $t = 100s$ with parameters $r_{\delta} = 0.79 + 0.05\sin(0.1t)$, $r_{\phi} = 0.75 + 0.03\cos(0.2t)$, $d_{\delta} = 0.09 + 0.06\sin(0.1t)$, $d_{\phi} = 0.08 + 0.02\cos(0.2t)$. The multiple model uncertainties include -30% deviations of aerodynamic parameters, the time-varying mass and inertia with parameters $m = m_0(0.8 + 0.2e^{-0.03t})$, $I = I_0(0.8 + 0.2e^{-0.03t})$, and the external disturbances with parameters $d_{T_e} = 30 + 6\sin(0.03t)$, $d_{D_e} = 26\sin(0.05t)e^{-0.05t}$, $d_{L_e} = 30 + 15\cos(0.045t)$, and $d_{M_e} = 300 + 65\cos(0.045t)$. The measurement noises are injected into the measurement signals.

The simulation results of Case 2 are presented in Figures 9–14. The velocity and altitude tracking performance are depicted in

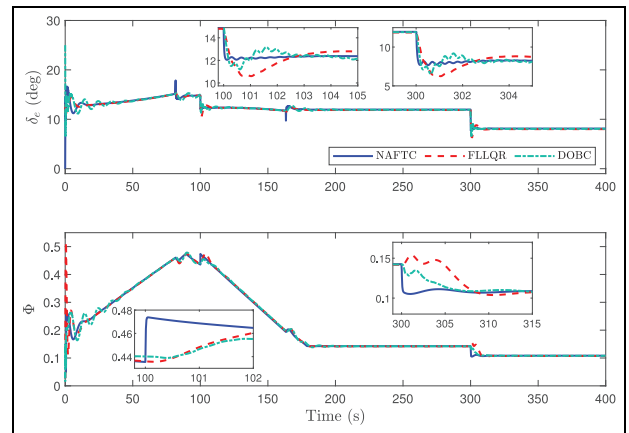


Figure 7. Control action in Case 1.

Figures 9 and 10. It is clear that the velocity and altitude of NAFTC accurately converge to the reference despite the time-varying actuator failures and multiple model uncertainties, while the two other comparison methods continue to fluctuate due to

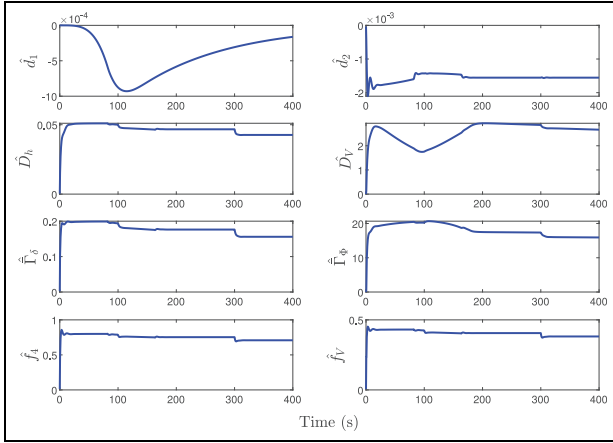


Figure 8. Estimation of disturbance observer and adaptive law in Case 1.

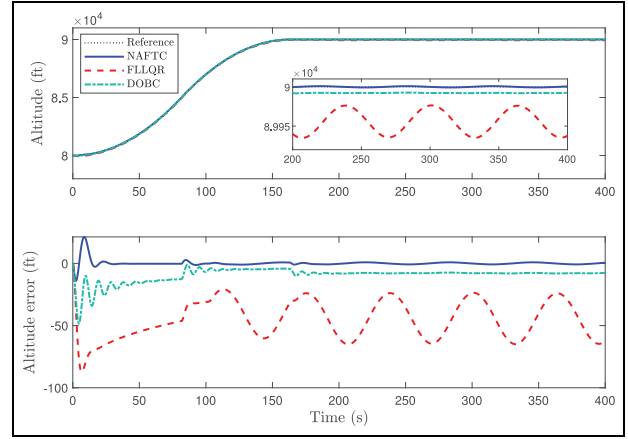


Figure 10. Altitude tracking performance in Case 2.

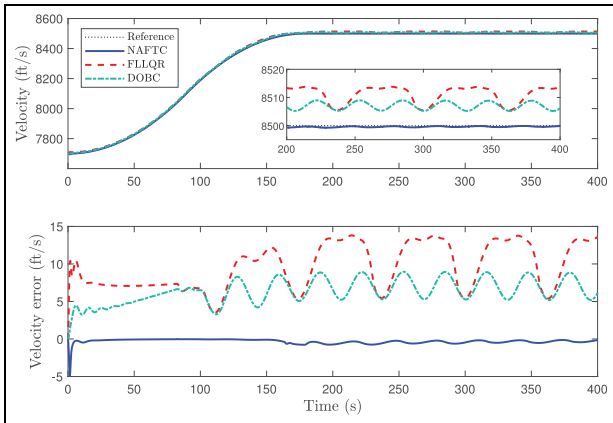


Figure 9. Velocity tracking performance in Case 2.

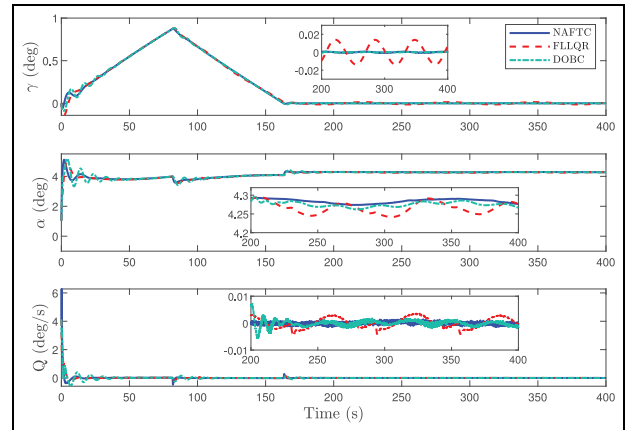


Figure 11. Attitude state in Case 2.

these adverse effects. Moreover, the velocity and altitude errors of NAFTC are less than those of the two other comparison methods. Specifically, the errors of NAFTC are less than 0.9ft/s and 2.8ft, respectively, when it comes to FLLQR are 13.8ft/s and 64.9ft, and DOBC are 8.9ft/s and 10.2ft. The attitude states are depicted in Figure 11. When time-varying actuator failures occur, there are fluctuations in the attitude states of FLLQR and DOBC, especially the fluctuation of FLLQR is violent, but NAFTC remains stable. In addition, from the third part in Figure 11, it can be observed that the measurement noises have a certain effect on the pitch angular velocity of NAFTC and DOBC, while FLLQR has almost no effect. But these negative effects can be ignored by considering the overall control performance. The elastic mode coordinates are depicted in Figure 12. The control actions are depicted in Figure 13, the control actions of all three methods are time-varying to compensate for time-varying actuator failures and multiple uncertainties. Nevertheless, according to the overall control effects, we can infer that the control actions of NAFTC are more effective and accurate. The estimation results of the disturbance observers and adaptive laws are depicted in Figure 14.

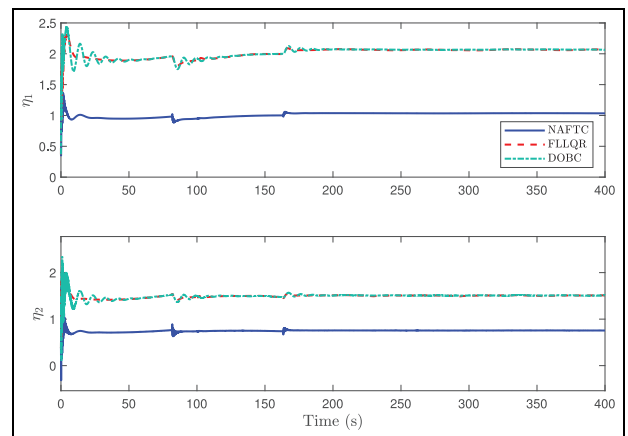


Figure 12. Elastic mode coordinate in Case 2.

In general, the simulation results verify that the NAFTC is capable of dealing with time-varying actuator failures and

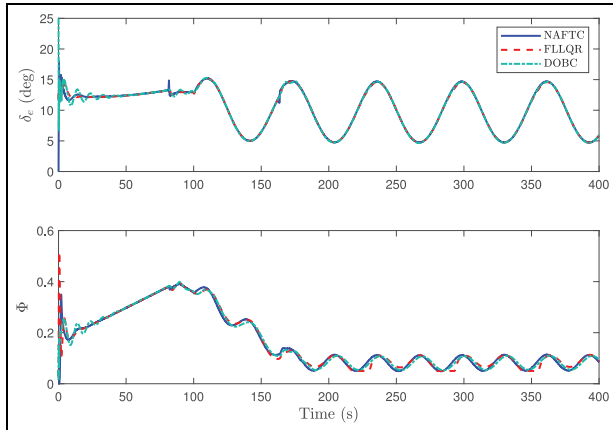


Figure 13. Control action in Case 2.

multiple model uncertainties. Moreover, the proposed method ensures uniform ultimate boundedness despite the actuator failures and multiple model uncertainties, which is consistent with the theoretical analysis.

Conclusion

In this paper, a disturbance observer-based neural adaptive fault-tolerant control method is proposed for FAHVs subject to contingent actuator failures and multiple model uncertainties. Based on the tracking differentiator and first-order filter, the smooth reference information for controller design is generated and the complexity of the recursive control framework is reduced. Then, the smooth reference information is combined with the smooth adaptive compensation control action using the tangent control function, ensuring that the flexible vibration is suppressed more effectively. Moreover, the time-varying actuator failures, aerodynamic deviations, and external disturbances are addressed utilizing the capable adaptive laws. Meanwhile, the neural networks are seamlessly combined with the adaptive control to handle the unknown models caused by the mass and inertia deviations. Finally, the simulations assess the tracking performance and robustness of the proposed method. The analysis indicates that NAFTC has more advantages than other control methods in terms of control accuracy, response agility for contingent actuator failures, and flexible vibration suppression ability.

Declaration of conflicting interests

The author(s) declared no potential conflicts of interest with respect to the research, authorship, and/or publication of this article.

Funding

The author(s) disclosed receipt of the following financial support for the research, authorship, and/or publication of this article: This work was supported, in part, by the National

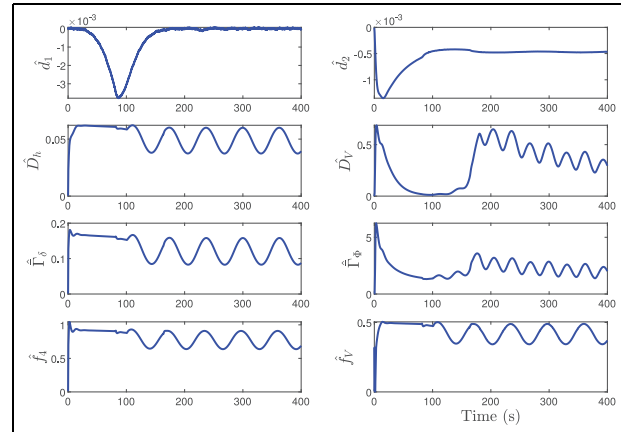



Figure 14. Estimation of disturbance observer and adaptive law in Case 2.

Key Research and Development Program of China No. 2019YFE0127000 and the Key Research and Development Project of Jilin Province No. 20210201015GX.

ORCID iD

Youyang Qu  <https://orcid.org/0000-0002-7336-285X>

References

- An H, Guo Z, Wang G, et al. (2021) Neural adaptive control of air-breathing hypersonic vehicles robust to actuator dynamics. *ISA Transactions* 116: 17–29.
- An H, Liu J, Wang C, et al. (2016) Disturbance observer-based anti-windup control for air-breathing hypersonic vehicles. *IEEE Transactions on Industrial Electronics* 63(5): 3038–3049.
- An H, Wu Q, Wang G, et al. (2020) Adaptive compound control of air-breathing hypersonic vehicles. *IEEE Transactions on Aerospace and Electronic Systems* 56(6): 4519–4532.
- Argha A, Su SW and Celler BG (2019) Control allocation-based fault tolerant control. *Automatica* 103: 408–417.
- Ding Y, Wang X, Bai Y, et al. (2019a) Global smooth sliding mode controller for flexible air-breathing hypersonic vehicle with actuator faults. *Aerospace Science and Technology* 92: 563–578.
- Ding Y, Wang X, Bai Y, et al. (2019b) Robust fixed-time sliding mode controller for flexible air-breathing hypersonic vehicle. *ISA Transactions* 90: 1–18.
- Guo J, Peng Q and Zhou J (2019a) Disturbance observer-based nonlinear model predictive control for air-breathing hypersonic vehicles. *Journal of Aerospace Engineering* 32(1): 04018121.
- Guo J, Zhang T, Cheng C, et al. (2019b) Model reference adaptive attitude control for near space hypersonic vehicle with mismatched uncertainties. *Transactions of the Institute of Measurement and Control* 41(5): 1301–1312.
- Guo Z, Guo J, Zhou J, et al. (2020) Robust tracking for hypersonic reentry vehicles via disturbance estimation-triggered control. *IEEE Transactions on Aerospace and Electronic Systems* 56(2): 1279–1289.
- Han J (2009) From PID to active disturbance rejection control. *IEEE Transactions on Industrial Electronics* 56(3): 900–906.
- He J, Qi R, Jiang B, et al. (2015) Adaptive output feedback fault-tolerant control design for hypersonic flight vehicles. *Journal of the Franklin Institute* 352(5): 1811–1835.

- He X, Ma Y, Chen M, et al. (2022) Flight and vibration control of flexible air-breathing hypersonic vehicles under actuator faults. *IEEE Transactions on Cybernetics*. Epub ahead of print 9 March 2022. DOI: 10.1109/TCYB.2022.3140536.
- Hu Y, Wu B, Geng Y, et al. (2019) Smooth time-optimal attitude control of spacecraft. *Proceedings of the Institution of Mechanical Engineers* 233(7): 2331–2343.
- Lavretsky E and Wise KA (2013) *Robust and Adaptive Control: With Aerospace Applications*. London: Springer.
- Parker JT, Serrani A, Yurkovich S, et al. (2007) Control-oriented modeling of an air-breathing hypersonic vehicle. *Journal of Guidance Control and Dynamics* 30(3): 856–869.
- Sachan K and Padhi R (2020) Nonlinear robust neuro-adaptive flight control for hypersonic vehicles with state constraints. *Control Engineering Practice* 102: 104526.
- Shao X, Shi Y and Zhang W (2021a) Fault-tolerant quantized control for flexible air-breathing hypersonic vehicles with appointed-time tracking performances. *IEEE Transactions on Aerospace and Electronic Systems* 57(2): 1261–1273.
- Shao X, Shi Y, Zhang W, et al. (2021b) Prescribed fast tracking control for flexible air-breathing hypersonic vehicles: An event-triggered case. *Chinese Journal of Aeronautics* 34(11): 200–215.
- Shi Y, Shao X and Zhang W (2020) Quantized learning control for flexible air-breathing hypersonic vehicle with limited actuator bandwidth and prescribed performance. *Aerospace Science and Technology* 97: 105629.
- Wang G, Liu K, Sun Z, et al. (2020) Attitude-orbit cooperative control for small-scale spacecraft with chemical propulsion: Adaptive sliding mode control based on neural network. *Journal of Aerospace Engineering* 33(6): 04020080.
- Wang L, Qi R and Jiang B (2022) Adaptive actuator fault-tolerant control for non-minimum phase air-breathing hypersonic vehicle model. *ISA Transactions* 126: 47–64.
- Wang N, Wu HN and Guo L (2014) Coupling-observer-based nonlinear control for flexible air-breathing hypersonic vehicles. *Nonlinear Dynamics* 78(3): 2141–2159.
- Wang Z and Yuan J (2019) Full state constrained adaptive fuzzy control for stochastic nonlinear switched systems with input quantization. *IEEE Transactions on Fuzzy Systems* 28: 645–657.
- Wang Z, Zhang B and Yuan J (2018a) Decentralized adaptive fault tolerant control for a class of interconnected systems with nonlinear multisource disturbances. *Journal of the Franklin Institute* 355(11): 4493–4514.
- Wang Z, Zhang B, Yuan J, et al. (2018b) Robust adaptive fault tolerant control for a class of linearly parameterized uncertain nonlinear systems: An integrated method. *Transactions of the Institute of Measurement and Control* 40(7): 2129–2140.
- Xu H, Mirmirani MD and Ioannou PA (2004) Adaptive sliding mode control design for a hypersonic flight vehicle. *Journal of Guidance Control and Dynamics* 27(5): 829–838.
- Young WH (1912) On classes of summable functions and their Fourier series. *Proceedings of the Royal Society of London. Series A, Containing Papers of a Mathematical and Physical Character* 87(594): 225–229.
- Zhang F, Meng D and Li X (2022) Robust adaptive learning for attitude control of rigid bodies with initial alignment errors. *Automatica* 137: 110024.
- Zhang X, Zong Q, Dou L, et al. (2020) Improved finite-time command filtered backstepping fault-tolerant control for flexible hypersonic vehicle. *Journal of the Franklin Institute* 357(13): 8543–8565.

Appendix A

Notation

$C_{(\cdot)}^{(\cdot)}, \beta_i$	aerodynamic coefficients by curve fitting
$d_{T_e}, d_{D_e}, d_{L_e}, d_{M_e}$	external disturbance force and torque
h	altitude (ft)
m, I	mass and inertia
M	pitching torque
q	pitch angular velocity, PAV (rad/s)
\bar{q}, g	dynamics pressure and gravitational acceleration
S, \bar{c}	reference area and mean aerodynamic chord
T, D, L, N_1, N_2	thrust, drag, lift-force and elastic force
V	velocity (ft/s)
$ x $	absolute value of x
\bar{x}	upper bound of $ x $
$\ x\ ^2$	norm of vector x
z_T	coupling between T and M (ft)
α	angle of attack, AOA (rad)
γ	flight path angle, FPA (rad)
δ_e	elevator deflection (rad)
$\Delta(\cdot)$	unmodeled and uncertainties of the aerodynamic force and torque
η_1, η_2	generalized elastic mode coordinate
ξ_1, ξ_2	damping coefficient of elastic dynamics
Φ	fuel equivalence ratio
$\tilde{\psi}_1, \tilde{\psi}_2$	rotational coupling coefficient of elastic mode
ω_1, ω_2	frequency coefficient of elastic dynamics